JOURNAL OF Applied Polymer SCIENCE

Structure–Property Correlation of Polyurethane Nanocomposites: Influence of Loading and Nature of Nanosilica and Microstructure of Hyperbranched Polyol

Pradip K. Maji,[1] Anil K. Bhowmick[1,2]

[1]Rubber Technology Centre, Indian Institute of Technology, Kharagpur 721302, India

[2]Indian Institute of Technology, Patna 800013, India

Correspondence to: A. K. Bhowmick (E-mail: anilkb@rtc.iitkgp.ernet.in) or (E-mail: director@iitp.ac.in)

ABSTRACT: New generation polyurethane nanocomposites based on toluene diisocyanate, poly(propylene glycol), hyperbranched polymers (HBPs), and nanosilica were synthesized with the aim of determining the effect of the loading and nature of nanosilica and the functionality of HBP on the structure and properties of polyurethane nanocomposites. Good dispersion of nanosilica at 4 wt % loading in the polymer was confirmed from atomic force microscopy. The properties of the polyurethane nanocomposites were a function of content and nature of the nanosilica in the matrix. The optimum silica loading was 4 wt %. At this loading, tensile strength and storage modulus at 25°C of the nanocomposites increased by 52 and 40%, respectively over the pristine polyurethane. Organo-treated nanosilica exhibited higher physico-mechanical properties than the untreated one. With the increase of functionality in the hyperbranched polyol, the tensile strength, thermal stability, and dynamic mechanical properties of the nanocomposites improved.
 J. Appl. Polym. Sci. 000: 000–000, 2012

KEYWORDS: polyurethane; nanocomposites; nanosilica; hyperbranched polymer

Received 27 March 2011; accepted 9 May 2012; published online

DOI: 10.1002/app.38063

INTRODUCTION

The field of polymer-based nanocomposites is one of the most admired areas in current polymer research and developments. Polymer nanocomposites have attracted considerable awareness and worldwide importance during the last decade. In recent years, a great deal of attention has been paid to the preparation of polymer/nanometer-sized inorganic nanocomposites due to their striking mechanical, thermal, dynamic-mechanical, optical, magnetic and electrical properties, and potential applications.[1–6] The reinforcing inorganic elements are usually composed of either layered clays, or spherical silica particles. A huge number of studies associated with exfoliation of layered silicates have been carried out,[7–10] but the papers dealing with polymer nanocomposites reinforced with dispersed silica nanoparticles are few. This is due to the fact that the specially prepared nanoparticles are required to defeat attractive forces between them that guide to their agglomeration.

The properties of a nanocomposite are greatly influenced by degree of dispersion of nanoparticles in a base polymer and interfacial adhesion between inorganic and organic components.[11] The most challenging task is to disperse nanoparticles into a polymer matrix, as these tend to agglomerate. In the case of silica nanoparticles, the presence of hydroxyl groups can lead to hydrogen bonding and form a continuous structure. Though nanocomposites can be made by blending of nanoparticles with base polymers by means of high shear stirring, the degree of dispersion of nanoparticles and the interfacial adhesion are obviously inadequate to impart attractive material properties.[12] As a result, several chemical approaches are adopted for the preparation of nanocomposites in current years. Surface modification is one of the processes to reduce the agglomeration tendency of the nanosilica particles.[13] The aim is to reduce the high surface energy and particle interactions. Wu et al.[14] have reported the surface treatment of nanosilica for preparation of polypropylene–silica nanocomposite. This is the first time that we have reported the hyperbranched polyurethane nanocomposites containing modified and unmodified nanosilica as reinforcement agent.

Polyurethane is one of the most commonly used polymers for different applications as hard plastic to soft rubber to liquid resin.[15–17] It is versatile from its chemistry point of view. Polyurethane is generally formed from the reaction of a polyol and a diisocyanate. By varying the structure and degree of functionalization of the starting materials, a wide range of polyurethane products can be obtained.[16] Polyurethane generally consists of

soft segments, which are high molecular weight polyester or polyether macrodiol, and the hard segments, which are composed of diisocyanate and low molecular weight diol or diamine.[17] The exceptional properties of PU are due to microphase separation that takes place during the reaction between the isocyanate groups and the hydroxyl functionalities of polyol.

Recent development of synthetic procedures has made functionalized dendrimers readily available in large quantities to facilitate rapid development of dendrimer chemistry.[18–21] The highly branched macromolecules investigated here are comprised of hyperbranched polymers (HBPs), which have a tree-like structure with a large number of branch points radiating from a multifunctional core molecule, and hence a potentially high degree of end-group functionality per molecule. Currently, we are developing PU of varying micro- and nanostructure from various hyperbranched polymers.[22] Polymerization of PU prepolymer with polyester HBPs in presence of nanosilica may provide a means of obtaining nanocomposites without aggregation. Until now, there are only a few literature references[23] on PU silica nanocomposites having hyperbranched polymer. A huge gap is also present in the literature references on PU based on hyperbranched polymer and their silica nanocomposites.

The uniqueness of the present research is that crosslinked polyurethanes having different microstructure at various loadings of nanosilica have been successfully synthesized and characterized. Thus, the present study can reveal how the microstructure of hyperbranched polymer and nature and loading of nanosilica influence the morphology and properties of the polyurethane matrix. This is the first time we have prepared the unique polyurethane–silica nanocomposites with different microstructure of both the polymer and the filler and established a structure–property correlation.

A series of network structure has been synthesized in bulk by varying the microstructure of hyperbranched (HB) polyols (here 2nd, 3rd, and 4th generation HB polyol) as crosslinker from polyurethane prepolymer stage. The total reaction scheme is given in Figure 1. Amount of ingredients for the synthesis of stoichiometric system was calculated from the number of —OH groups in the crosslinker and —NCO groups present in the prepolymer. The detailed synthesis, characterization, and evaluation of properties of PU and its nanocomposites have been described in the Experimental section. Relationship between morphology and properties has been discussed here in this article.

EXPERIMENTAL

Materials

Polypropylene glycol (PPG) of molecular weight 2000 was procured from Sigma–Aldrich Chemicals, Bangalore, India. Toluene 2, 4-diisocyanate was purchased from Merck Schuchardt OHG, Germany. Nanosilica used was Aerosil®200, Aerosol®300, Aerosil®R805, and Aerosil®R812S from Degussa GmbH, Germany. According to the supplier, Aerosil®R805 is a nanosilica after treatment with an octylsilane on Aerosil®200 and Aerosil®R812S is a nanosilica treated with 1,1,1,3,3,3-hexamethyldisiliazane (HMDS) on Aerosol®300.[24] The detail physico-mechanical properties of all the nanosilica are given in Table I. Nanosilica was further characterized by FTIR spectroscopy and transmission electron microscopy. Dibutyltin dilaurate (DBTL) was procured from Aldrich Chemicals, Bangalore, India. Dry solvent, tetrahydrofuran (THF) was purchased from Rankem, Kolkata, India. Second generation (H20), third generation (H30), and fourth generation (H40) hyperbranched polyester (HBP) polyol were procured from Perstorp Specialty Chemicals, AB, Sweden. The structure of the hyperbranched polymers is shown in Figure 1. Detail characteristic properties were given in our previous paper.[22]

Synthesis of PU Prepolymer

The polyurethane prepolymer was synthesized in nitrogen atmosphere by reacting 2 mole of TDI with 1 mole of polypropylene glycol at 80°C in a round bottom flask (500 cm^3) with continuous stirring. The reaction scheme is given in Figure 1. The exothermic reaction was controlled by cooling and the temperature was maintained at 80°C. The isocyanate (—NCO) concentration in prepolymer reached a constant value after 4 h. The isocyanate content in the prepolymer was 4.4%, which was determined by the titrametric method. The viscosity of the prepolymer determined by ASTM part 22D-1084 (1984) was found to be 2480 poise. The molecular weight determined by GPC method was 2200 g $mole^{-1}$. Proper precaution was taken during the handling of TDI due to its toxicity.

Synthesis of Nanocomposites

For the preparation of the nanocomposite, the prepolymer was reacted with three types of hyperbranched polyol material (H20, H30, and H40) separately. An equivalent amount of branched polyol was added (equivalent ratio of —NCO: —OH = 1 : 1) to the diluted prepolymer in THF with constant stirring at room temperature (25°C) in presence of 0.001 mole of DBTL catalyst. To investigate the effect of loading of nanosilica on the mechanical and thermal properties, and micro structure of the polyurethane–nanosilica nanocomposite, three concentrations of nanosilica were used: 2.0, 4.0, and 8 wt %. The nanosilica was dispersed first in THF in a beaker (2% w/v) by ultrasonicator and finally added to the matrix with constant stirring. The samples for mechanical and thermal properties were prepared by casting the solution in a circular quartz mould and the thickness was adjusted by the amount of the cast solution. Pure PU was also synthesized by the same procedure without addition of nanoparticles. The designations of different nanocomposite samples are given in Table II.

CHARACTERIZATION

Fourier Transform Infrared (FT-IR) Spectroscopic Studies

FTIR of silica powder was done by preparing KBr plates by taking 1 : 4 silica and KBr using Perkin Elmer FTIR—spectrophotometer (model spectrum RX I), within a range of 400–4400 cm^{-1} using a resolution of 4 cm^{-1}. An average of 16 scans was reported for each sample.

Transmission Electron Microscopy (TEM)

A JEOL JEM-2010 instrument was used to analyze the morphology of the nanosilicas and nanocomposites; an acceleration voltage of 120 kV was used. The nanosilicas were placed directly by solvent casting into the grid specially designed for TEM analysis. For nanocomposites, the samples for TEM analysis were prepared by ultracryomicrotomy with a Leica Ultracut UCT (Leica

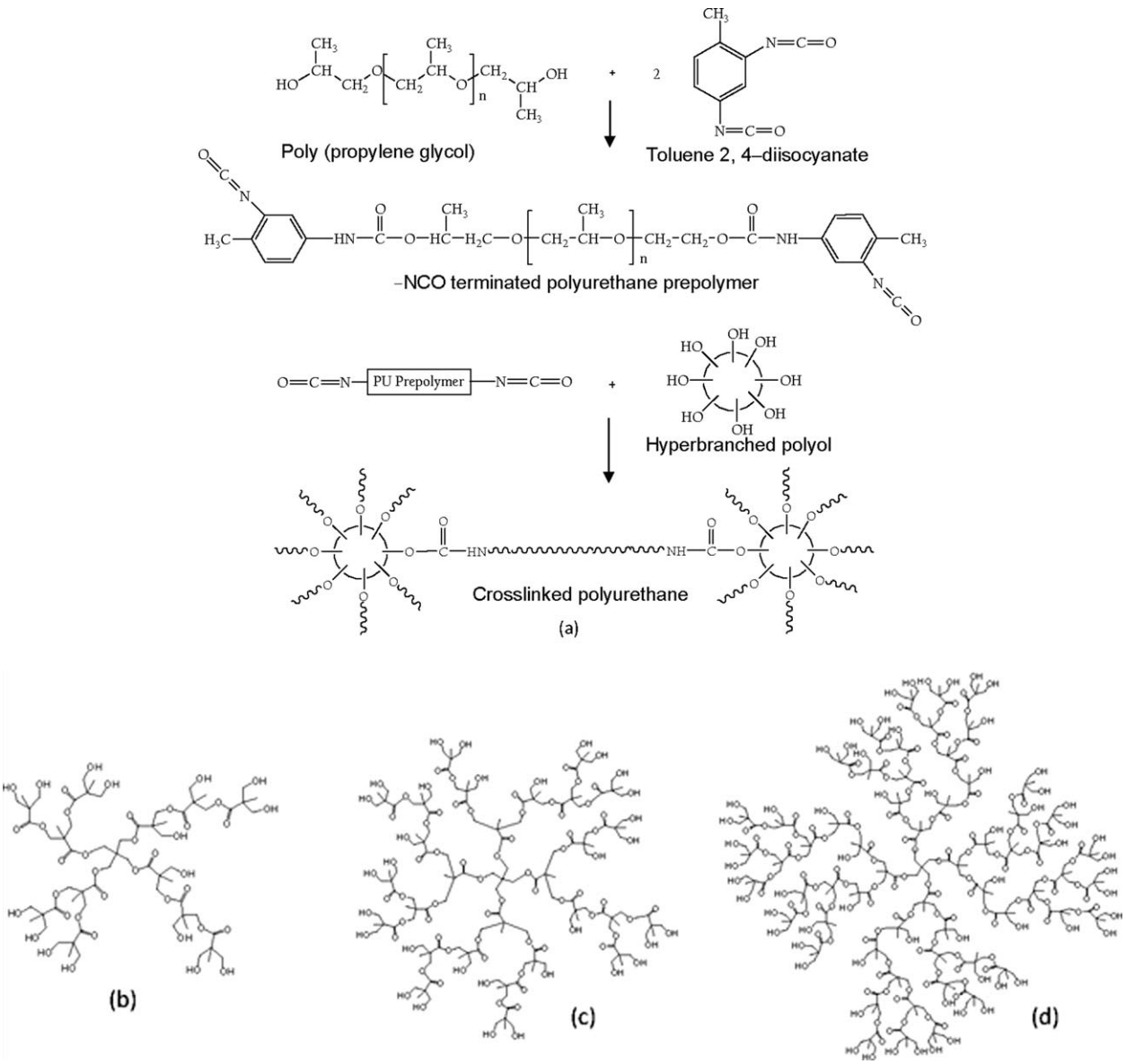

Figure 1. (a) Reaction scheme of the crosslinking of polyurethane prepolymer with hyperbranched polyol; (b) Chemical structure of 2nd generation hyperbranched polyol; (c) Chemical structure of 3rd generation hyperbranched polyol; (d) Chemical structure of 4th generation hyperbranched polyol.

Mikrosystems GmbH, Vienna, Austria). Freshly sharpened glass knives with cutting edges of 45° were used to obtain cryosections of 50–70 nm thickness. Because these samples were elastomeric in nature, the sample and glass knife temperatures during ultracryomicrotomy were kept constant at −50 and −60°C, respectively [these temperatures were well below the glass transition temperature (T_g) of PUs]. The cryosections were collected individually in a sucrose solution and directly supported on a copper grid of 300-mesh size.

Atomic Force Microscopy

Multimode scanning probe microscope with a Nanoscope IIIa controller by Digital Instruments (Veeco Metrology Group), Santa Barbara, CA was used for the atomic force microscopy (AFM) studies. The AFM measurements on the surface of the cast cured polyurethane samples were carried out in air at ambient conditions (25°C) using tapping mode probes with constant amplitude (40 mV). The rotated tapping mode etched silicone probe (RTESP) [square pyramid in shape with a spring constant of 20 N m^{-1}, nominal radius of curvature of 10 nm] with resonance frequency of 270 kHz was used. Phase images were recorded simultaneously at the resonance frequency of the cantilever with a scan rate of 1 Hz and a resolution of 256/512 samples per line. This allowed resolution of individual primary block morphology measurements. The images were analyzed using a nanoscope image processing software (5.30r1).

X-ray Diffraction (XRD) Studies

The XRD patterns of the samples were recorded in a Philips X-ray diffractometer (model PW-1710) at crystal monochromated

Table I. Physico-Chemical Data for Different Nanosilica

	Aerosil®			
Properties	200	300	R805	R812S
Avg. primary particle size (nm)	12	7	12	7
Carbon content (wt %)	0	0	4.5–6.5	3.0–4.0
Tapped density (approx. value) (acc. to DIN EN ISO 787/11, Aug. 1983) (g L^{-1})	50	50	60	60
Moisture content (2 h at 105°C) (wt %)	≤1.5	≤1.5	≤0.5	≤0.5
Ignition loss (2 h at 1000°C based on material dried for 2 h at 105°C) (wt %)	≤1.0	≤2.0	5.0–7.0	5.0–7.0
SiO_2-content (based on ignited material) (wt %)	≥99.8	≥99.8	≥99.8	≥99.8

Co Kα radiation in the angular range 5–50° (2θ) at 40 kV operating voltage and 20 mA current.

Volume Fraction of Rubber in the Swollen Gel

Previously weighed samples were allowed to swell in THF at 30°C for 24 h, the equilibrium swelling time (which was determined from a plot of mass uptake against time). The test pieces were then taken out, weighted, and then dried to a constant weight in a vacuum oven at 70°C for 6 h. The volume fraction of the rubber in the swollen gel (V_r) was determined on the basis of simple additive rule of volumes as follows [eq. (1)]:

$$V_r = \frac{(D - FH)/\rho_r}{(D - FH)/\rho_r + A_o/\rho_s} \quad (1)$$

where, H = weight of the test specimen; D = deswollen weight of the test specimen; F = weight fraction of the insoluble components; A_o = weight of the absorbed solvent; ρ_r = density of the rubber; ρ_s = density of the solvent.

Kraus Plot

Polymer–filler interaction in these nanocomposites was examined by using the Kraus plot,[25] as given below:

$$\frac{V_{r0}}{V_{rf}} = 1 - m\left(\frac{\phi}{1-\phi}\right) \quad (2)$$

where V_{r0} is the volume fraction of the polymer in the swollen gum; $V_{rf,}$ volume fraction of the polymer in the swollen filled system; and ø is the volume fraction of the filler in the filled nanocomposites.

Dynamic Mechanical Thermal Analysis (DMTA)

The dynamical mechanical thermal spectra of the samples were obtained by using DMTA of TA instruments (model 2980 V 1.7B). The sample specimens (30 mm × 6.2 mm × 0.7 mm) were analyzed in tensile mode at a constant frequency of 1 Hz, a strain of 0.01%, and a heating rate of 2°C min^{-1}. The data were analyzed by a TA Universal analysis software on TA computer attached to the machine. Storage modulus (E') and loss tangent (tan δ) were measured as a function of temperature for all the samples under identical conditions. The temperature corresponding to the peak in the tan δ versus temperature plot was taken as the glass–rubber transition temperature (T_g).

Thermogravimetric Analysis

Thermogravimetric analysis was done using Perkin–Elmer Instrument, Diamond TG-DTA. The samples (3–5 mg) were heated from ambient temperature to 800°C in the furnace of the instrument under air atmosphere at 60 mLmin^{-1} at a heating rate of 20°C min^{-1}. Analysis of the derivative thermogravimetric (DTG) curves was done and the onset temperature, weight loss at major degradation steps, and the temperature corresponding to the maximum degradation in the derivative thermogram were recorded. The temperature at which maximum degradation took place is denoted as T_{max} and the corresponding onset temperature of degradation (5%

Table II. Sample Description

Sample designation	Type of curing agent	Type of nanosilica	Amount of nanosilica in phr (parts per hundred)
$PU_{30}300_0$	3rd generation hyperbranched polyol	Aerosol®300	0
$PU_{30}300_2$	3rd generation hyperbranched polyol	Aerosol®300	2
$PU_{30}300_4$	3rd generation hyperbranched polyol	Aerosol®300	4
$PU_{30}300_8$	3rd generation hyperbranched polyol	Aerosol®300	8
$PU_{30}200_4$	3rd generation hyperbranched polyol	Aerosil®200	4
$PU_{30}805_4$	3rd generation hyperbranched polyol	Aerosil®R805	4
$PU_{30}812_4$	3rd generation hyperbranched polyol	Aerosil®R812S	4
$PU_{20}812_4$	2nd generation hyperbranched polyol	Aerosil®R812S	4
$PU_{40}812_4$	4th generation hyperbranched polyol	Aerosil®R812S	4

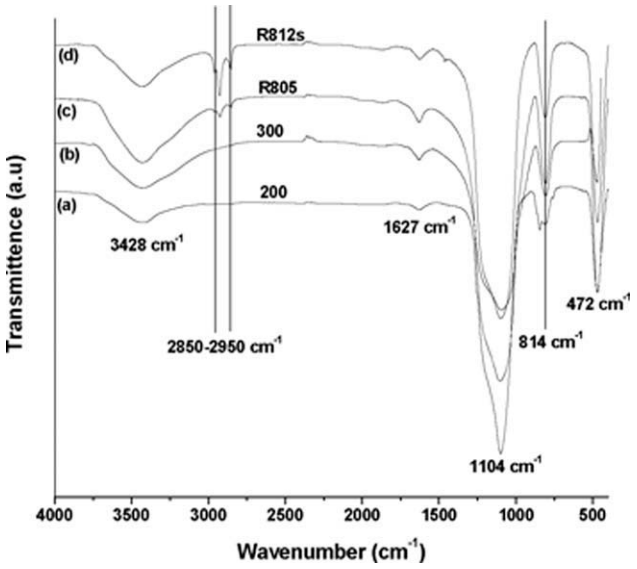

Figure 2. FTIR spectra of different nanosilicas (a) Aerosil®200, (b) Aerosil®300, (c) Aerosil®R805, and (d) Aerosil®R812S.

degradation) is represented as T_i. The error in the measurement was ±1°C.

Tensile Properties

Tensile specimens were punched out from the cast sheets using ASTM Die-C. The tests were carried out as per ASTM D 412-98 method in a Universal Testing Machine (Zwick 1445) at a crosshead speed of 500 mm min^{-1} at 25°C. The average of three tests is reported here.

RESULTS AND DISCUSSION

Characterization of the Nanosilicas

FTIR spectra give qualitative information on the surface treatment of the nanosilica particles. The spectra of the untreated (Aerosil®200 and 300) and the treated (Aerosil®R805 and R812S) silicas are shown in Figure 2. The spectrum of the four nanosilicas is relatively similar and shows a broad peak centered at about 3428 cm^{-1} and a small peak at 1627 cm^{-1}, which can be assigned to O—H stretching vibration of the surface silanol group. The FTIR spectrum exhibits strong Si—O—Si absorptions at about 1104 and 472 cm^{-1}, and also displays a weak Si—OH peak at 814 cm^{-1}. From the results of the treated nanosilica [Figure 2(c–d)], it can be observed that the new bands appear in the region of 2850–2950 cm^{-1} for —CH_3 and CH_2 stretching frequencies. These facts indicate that the modifier molecules have been successfully grafted onto the surfaces of the nanosilica particles (for the case of Aerosil®R805 and R812S). To investigate the interaction of silane with nanosilica, we have done the FTIR analysis after washing the silane grafted nanosilica with distilled water thee to four times. The results are same. The grafting of silane agents has been further confirmed from the supplier's data sheet.[24]

Figure 3 demonstrates the TEM micrographs of the silica nanoparticles. From the figure, it is shown that all silica nanoparticles have a primary particle size in the nanometer scale and have tendency to agglomerate. But this tendency decreases with the surface modification of the silica nanoparticles, as shown in Figure 3(c, d). This is likely due to less H-bonding in the case of surface treated nanosilicas.

Morphology of Polyurethane-Silica Nanocomposites by Atomic Force Microscopy (AFM)

Atomic force microscopy (AFM) has been used to investigate the dispersion of different nanosilica from the freshly cut surface of silica nanocomposites. Phase images of the samples from the bulk reveal different morphologies of the nanocomposites prepared. Some representative micrographs are given in Figures 4 and 5. Figure 4 shows the AFM morphology of the PU_{30} nanocomposites having 2, 4, and 8 wt % untreated nanosilica (Aerosil®300) loading. The brighter points in the images represent individual silica particles, whereas the darker area is for the polymer matrix. The micrographs show homogeneous dispersion of silicate layers in the polymer matrix up to 4 wt % nanosilica loading [Figure 4(b)]. Figure 4(c) exhibits the morphology of $PU_{30}300_8$ having 8 wt % of nanosilica loading. The image shows agglomeration of nanosilica throughout the PU matrix instead of dispersion. Dispersion of nanosilica in the PU matrix also depends on the nature of the nanosilica. Figure 5 shows the AFM micrograph at 4 wt % of modified silica loaded PU nanocomposites. Organo treated nanosilicas—Aerosil®R805 and R812S display better dispersion than the untreated nanosilica. Morphology of the other systems based on PU_{20} and PU_{40} follows the same trend. The best dispersion is observed in $PU_{40}812_4$.

Dispersion of the filler in the nanocomposites was analyzed and quantified by using ImageJ software as a tool.[26–28] Quantification of the extent of dispersion is attained by the dispersion parameter, $D_{0.1}$, which is defined as the free path distance distribution. This lies in the range of $0.9\bar{x}$ to $1.1\bar{x}$, where $\bar{x}$ is the mean spacing between the nanosilica particles. $D_{0.1}$ is a dimensionless quantity and is related to the extent of dispersion. A higher $D_{0.1}$ value indicates more data close to the value of mean spacing thereby suggesting better dispersion.[26–28] Free path distribution follows a lognormal distribution model[26] and $D_{0.1}$ is expressed as:

$$D_{0.1} = 1.1539 \times 10^{-2} + 7.5933 \times 10^{-2}(\bar{x}/s) + 6.6838 \times 10^{-4}(\bar{x}/s)^2 - 1.9169 \times 10^{-4}(\bar{x}/s)^3 + 3.9201 \times 10^{-6}(\bar{x}/s)^4 \quad (3)$$

where s is the standard deviation.

To estimate $D_{0.1}$, extensive measurements of the free path x_i (distance between the nanosilica particles) have been carried out. This is followed by calculation of $\bar{x}$ which is used in eq. (3) to calculate $D_{0.1}$.

Figure 6 is the representative plot of frequency versus distance between the nanosilica for PU nanocomposites at various filler loadings. The free path distance is calculated and the sampling number N is 260. The histogram showing the free path distance distribution is plotted in Figure 6. For all the nanocomposites, $D_{0.1}$ has been calculated and is tabulated in Table III. It is noticed that the threshold filler loading for this system is 4 wt

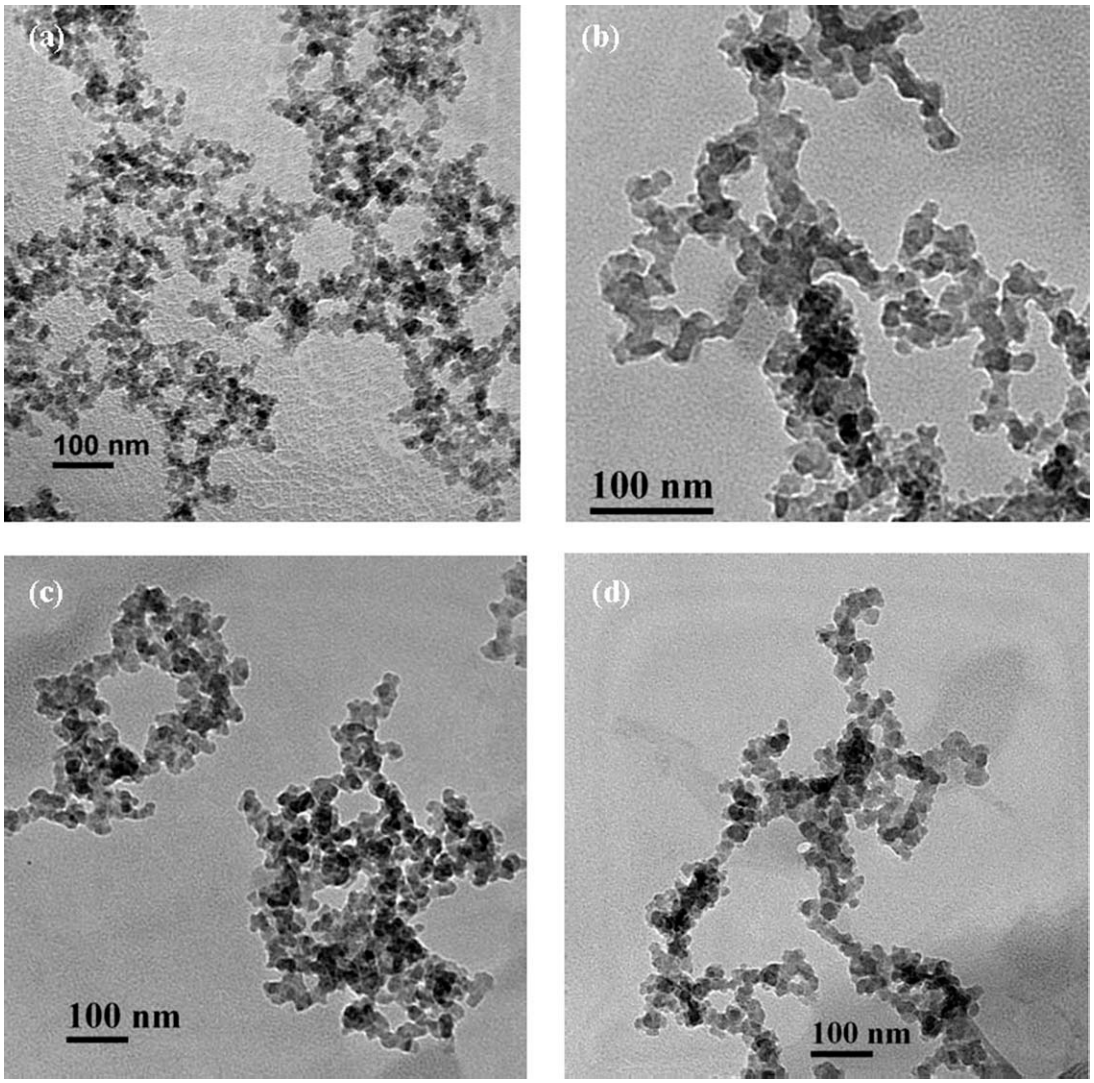

Figure 3. TEM photographs of different nanosilicas (a) Aerosil®300, (b) Aerosol®200, (c) Aerosil®R812S, and (d) Aerosil®R805.

%. With the modification of the filler, the dispersion parameter $D_{0.1}$ increases indicating the better dispersion of the modified fillers in polyurethane matrix. It is interesting to see that with an increase in the functionality in the hyperbranched polyol, the interaction parameter increases resulting in better dispersion of the filler in the polyurethane matrix. The result can be correlated with the three dimensional AFM images. Good dispersion is observed in $PU_{40}812_4$ as shown in Figure 7(c). It is in agreement with the calculation of dispersion parameter of different systems and polymer filler interaction parameter in the subsequent paragraph.

Figure 8 exhibits the tapping mode height images of some representative AFM photographs of nanosilica composites. The topological feature in the height image provides almost same kind of morphology of all nanocomposites. Interestingly, same circular architecture of the morphology in dark-bright contrast is obtained with height image of all the nanocomposites. There is a very less (~10 nm) height deviation in the image in Figure 8.

TEM Analysis

A representative TEM micrograph of polyurethane film of $PU_{30}300_4$ is shown in Figure 9 which indicates that most of the nanosilica particles are evenly dispersed at the scale of ~20–50 nm in the composite film, but some aggregates can still be observed. This is because nanosilica particles have much stronger hydrogen bonding through —OH groups. In most of the nanocomposites films, dispersion as well as agglomeration in places are observed. The agglomeration is negligible as compared to TEM photographs of pure nanosilicas.

X-ray Diffraction Analysis

WAXD shows significant change with loading and nature of nanosilica (Figure 10). There is a crystalline peak at 18.4° in the unfilled sample. This peak persists for all the nanocomposites. By contrast, in the Areosil 300 series of nanosilca composites, there is a clear effect of the nanospheres on the crystalline component (Figure 10). At zero loading, the crystalline peak at 18.4° is clear. This feature progressively weakens and broadens with loading with nanosilica. These results are consistent with

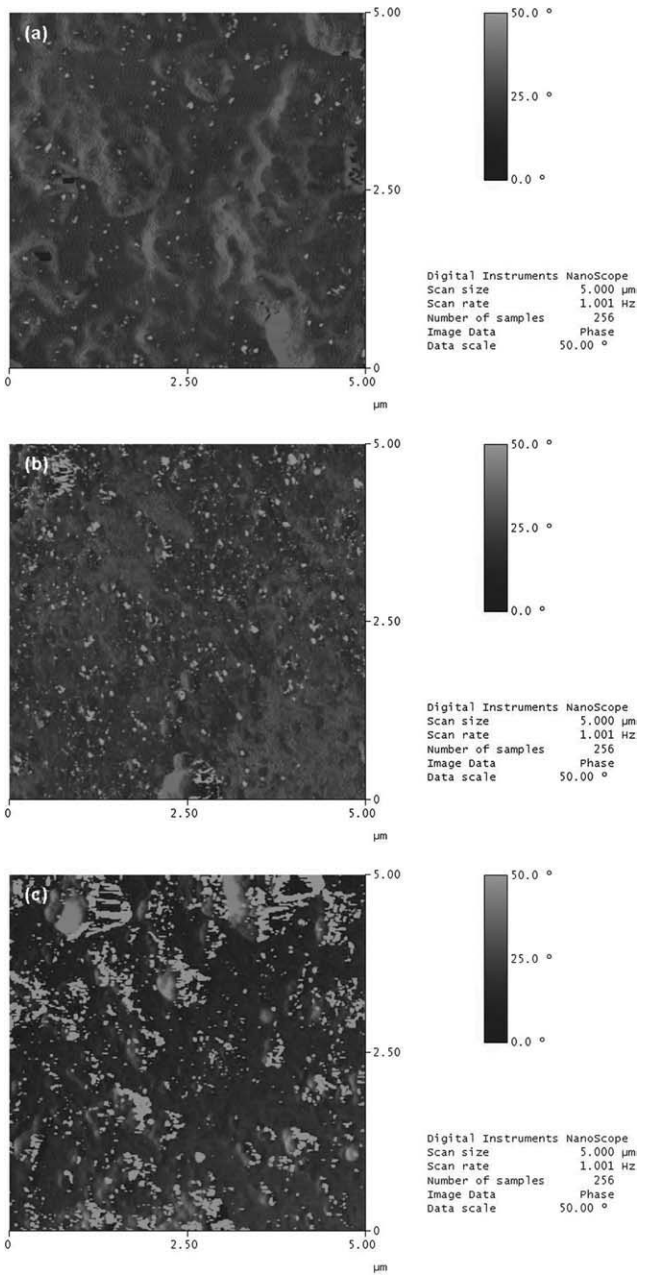

Figure 4. Phase image of AFM micrographs of different PU nanocomposites with nanosilica loading (a) $PU_{30}300_2$, (b) $PU_{30}300_4$, and (c) $PU_{30}300_8$.

the AFM and TEM analysis. There are interactions of the fillers with the polymer and consequently dispersion takes place that reduces crystalline domains in the PU matrix. The detailed polymer–filler interactions are given in next paragraphs. The interaction is maximum for Areosil 812 nanosilica with the PU matrix.

Polymer–Filler Interaction

Figure 11 shows the comparative Kraus plots [employing eq. (2)] for the polyurethane/silica organic–inorganic hybrid nanocomposites. A linear decrease of V_{r0}/V_{rf} with [ø/ (1 − ø)] is observed with all the hybrid nanocomposites; this decrease is especially larger for the modified silica hybrids compared with the other systems. Polymer–filler interaction in filled vulcanizates using Kraus plot has been reported,[29,30] but no early reports are available for the same on polyurethane nanosilica-based composites. V_{r0}/V_{rf} decreases with increase of [ø/(1 − ø)] irrespective of modification of filler (Figure 11); but for the modified silica systems, the decrease of V_{r0}/V_{rf} is significant because of high polymer–silica interaction. At the molecular level, interaction at the polymer–silica interface changes the molecular mobility. Swelling of the filled polymers is restricted by the presence of the filler. The polymer is adsorbed over the filler surface and changes the molecular weight distribution. The

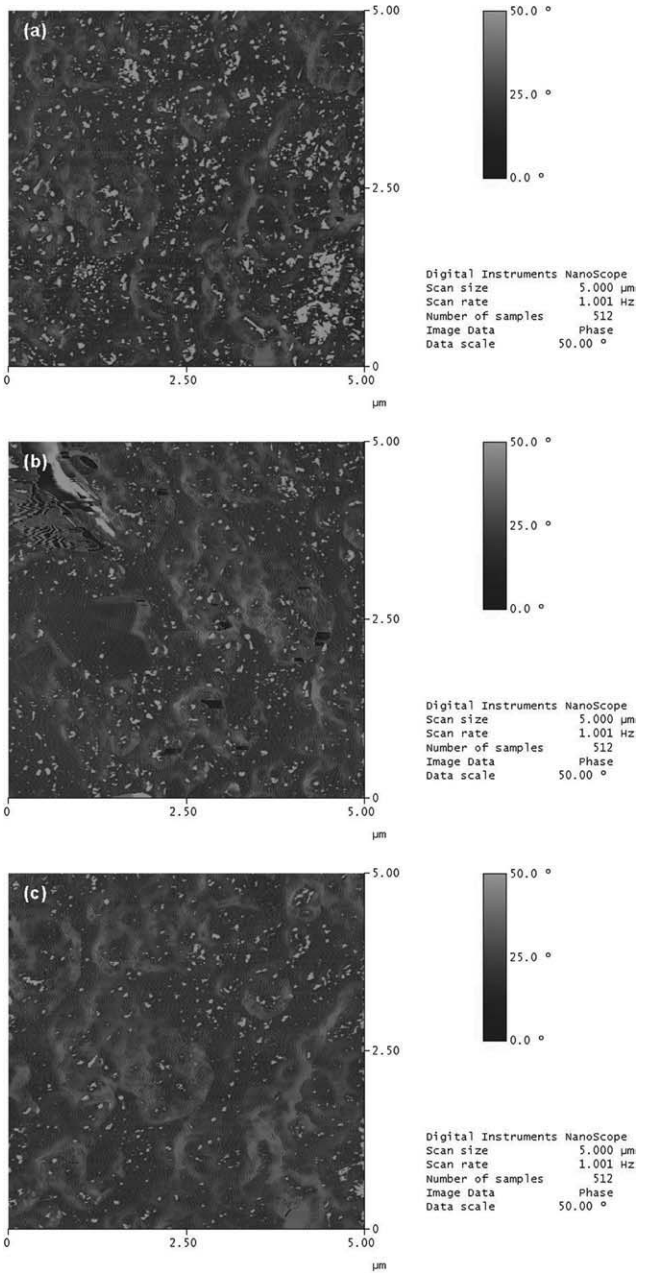

Figure 5. Phase image of AFM micrographs of different PU nanocomposites with different nanosilica (a) $PU_{30}805_4$, (b) $PU_{30}812_4$, and (c) $PU_{40}812_4$.

Applied Polymer SCIENCE

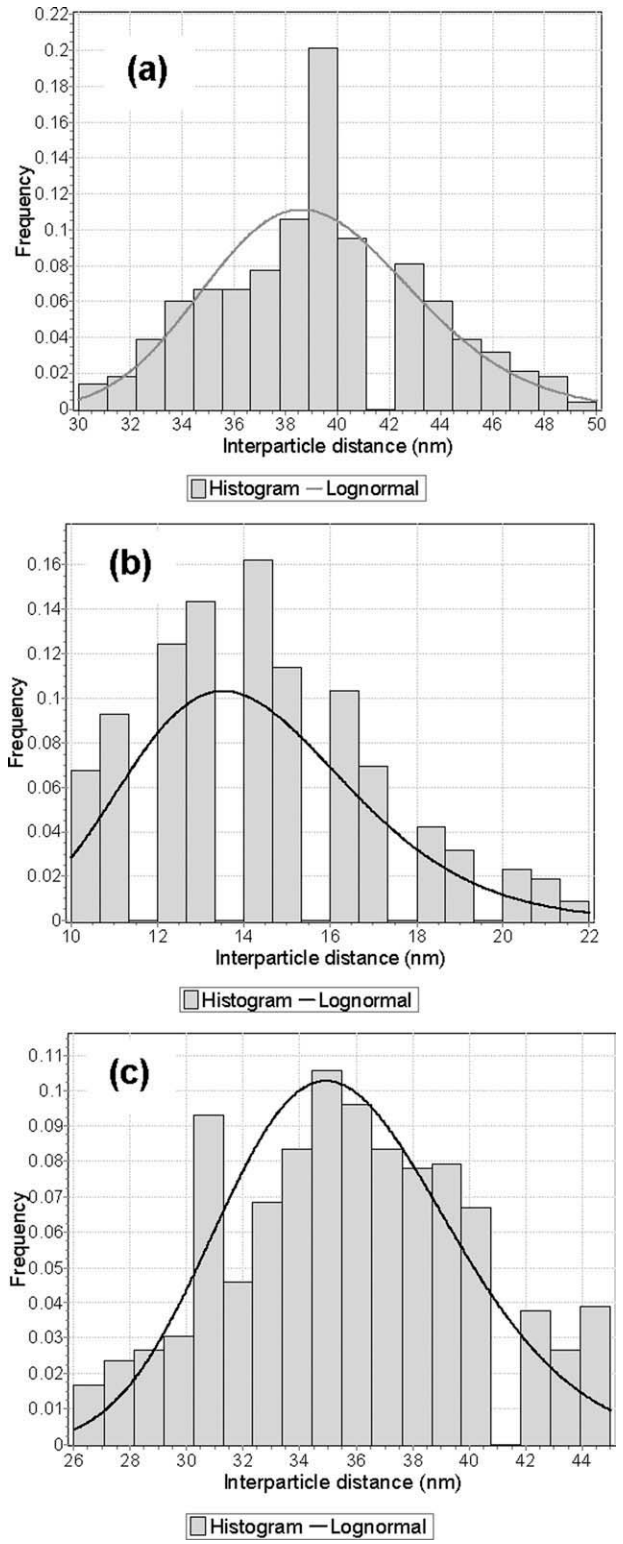

Figure 6. Plot of frequency versus distance between nanosilicas in different PU nanocomposite (a) $PU_{30}300_2$, (b) $PU_{30}300_8$, and (c) $PU_{40}300_4$.

extent of adsorption of the polymer over the filler is strongly related to the interactions between the filler and the matrix polymer, the surface area, and aggregation as well as concentration of the filler. It is seen that the $PU_{40}812_4$ has the lowest

Table III. Comparison of $D_{0.1}$ Values for Various Samples

Sample	$\bar{x}/s$	$D_{0.1}$ (%)
$PU_{30}300_2$	9.73	74
$PU_{30}300_4$	7.60	59
$PU_{30}300_8$	5.22	41
$PU_{30}200_4$	7.20	56
$PU_{30}805_4$	7.99	62
$PU_{30}812_4$	8.12	64
$PU_{20}812_4$	7.80	61
$PU_{40}812_4$	8.65	67

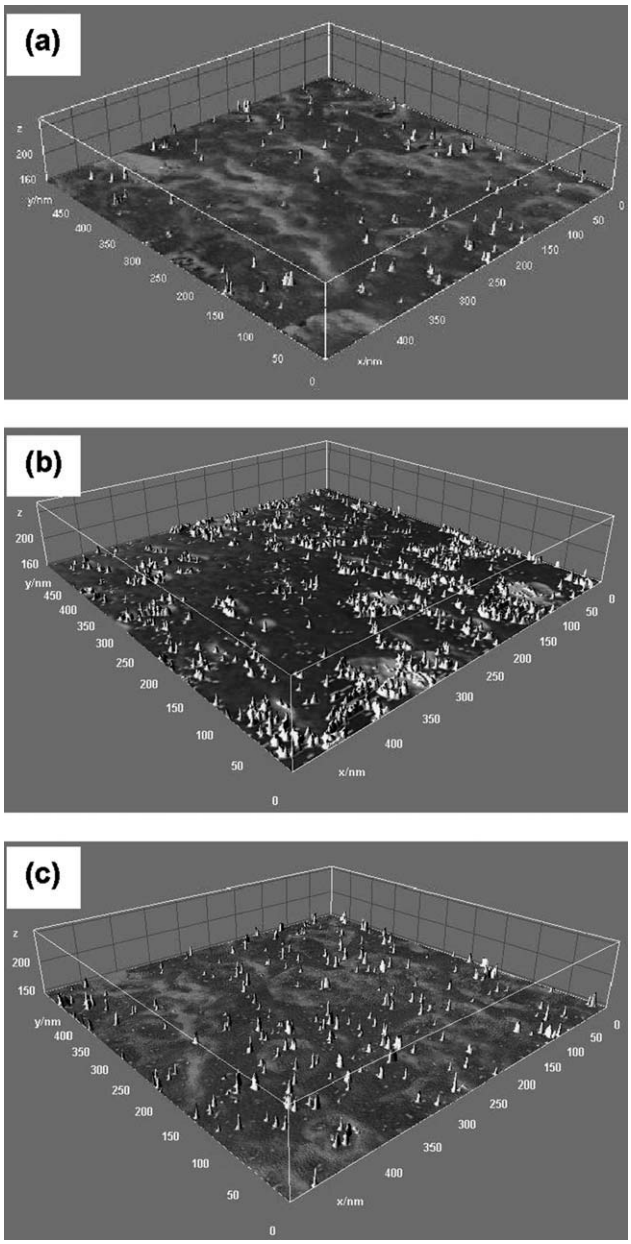

Figure 7. Three dimensional images of representative AFM phase images using ImageJ Software of different PU nanocomposites (a) $PU_{30}300_2$, (b) $PU_{30}300_8$, and (c) $PU_{40}812_4$.

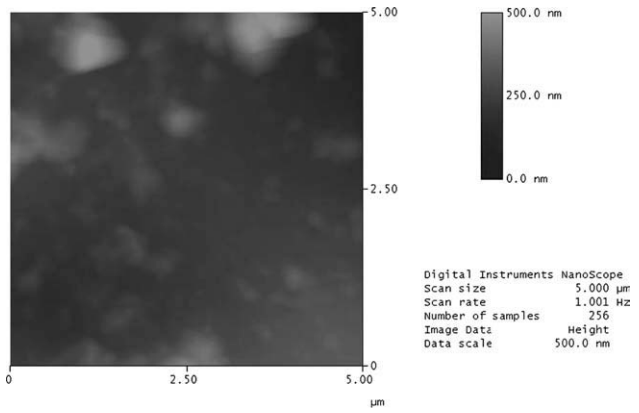

Figure 8. Representative height images of AFM micrographs of $PU_{30}300_2$.

value in the Kraus plot among all the systems indicating greater interaction between polyurethane matrix and the modified nanosilica. The results of Figures 5(c) and 7(c) are in accord with those of the Kraus plots.

Dynamic Mechanical Thermal Analysis (DMTA)

The viscoelastic properties of polyurethanes were characterized by using DMTA. The dissipation factor (tan δ) and storage modulus (E') curves are presented in Figures 12 and 13 for the representative samples and the data are given in Table IV. The tan δ peak is associated with the glass transition temperature (T_g) of the soft segment. The hard segment T_g is often difficult to detect in this type of PU,[31] and it is not clearly observed for any of the materials studied here. T_g is observed to increase in an approximately linear fashion with the increased addition of silica nanoparticles [Figure 12(a)]. The results are in agreement with those reported by Maji et al.[32] for clay polyurethane nanocomposites. For example, T_g for the neat PU ($PU_{30}300_0$) is −22°C, whereas the same for the nanocomposite having 4 wt % loading of nanosilica is −19°C. An approximately 3°C shift is observed with 4 wt % silica loading. The magnitude of the tan δ peak also decreases with an increase in the concentration of nanosilica, shown in the same figure. Mishra et al.[33] and

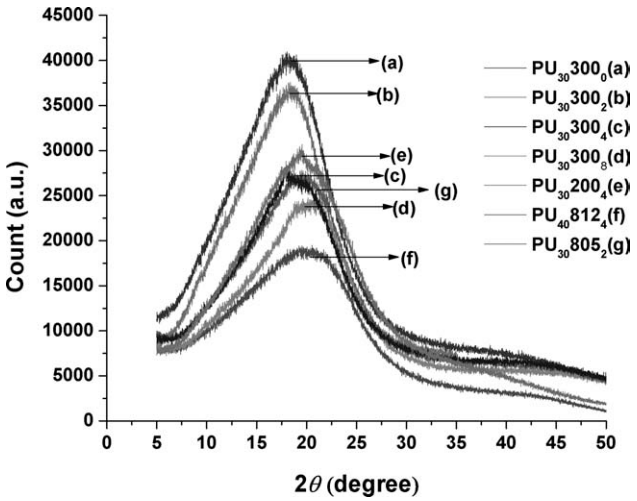

Figure 10. X-ray diffraction spectra of different nanocomposites.

Xiong et al.[34] reported the same trend for the linear PU nanocomposites with nanoclay loading. The tan δ peak for $PU_{30}300_0$ is observed at 0.62, which reduces to 0.48 for $PU_{30}300_4$. This is mainly attributed to good adhesion between the PU and the silica particles, as a result of which the nanometer-sized particles can restrict the segmental motion near the organic inorganic interface. This is applicable for all of the PUs. Nature of silica also plays a great role in the viscoelastic properties of PU–silica nanocomposites. Organo-treated silica shows a better result than that of untreated silica nanocomposites. From Figure 12(b), it is clear that the tan δ values of the treated silica nanocomposites are lower than that of the untreated ones. The best result is observed for $PU_{30}812_4$ system. This is in agreement with the AFM results in the earlier paragraph. As the size of the nanofiller decreases from 12 nm (for Aerosil®R805) to 7 nm (for Aerosil®R812S), more efficient polymer–filler interaction takes place due to the higher surface area of the later one. For the untreated silica nanocomposites, the same trend is observed [Figure 12(b)]. Another interesting phenomenon observed here is that with an increase in the functionality of the

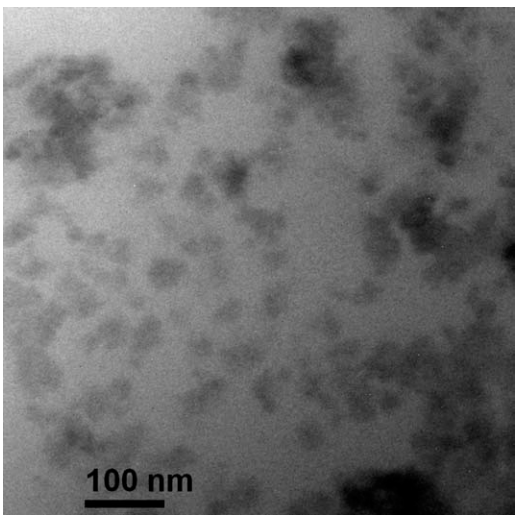

Figure 9. Representative TEM image of nanocomposits of $PU_{40}300_4$.

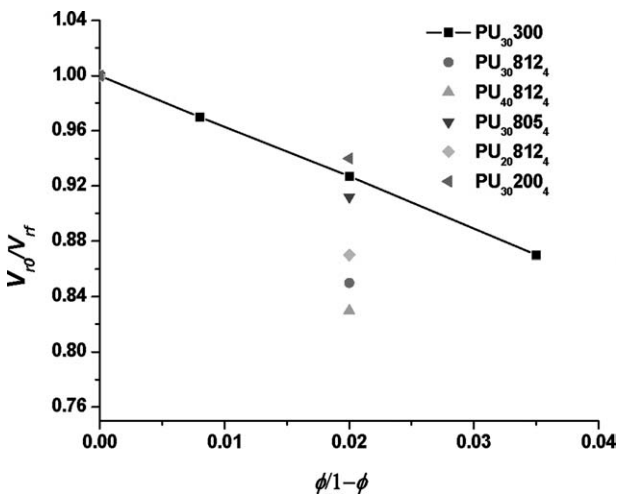

Figure 11. Kraus plot of different PU silica nanocomposites.

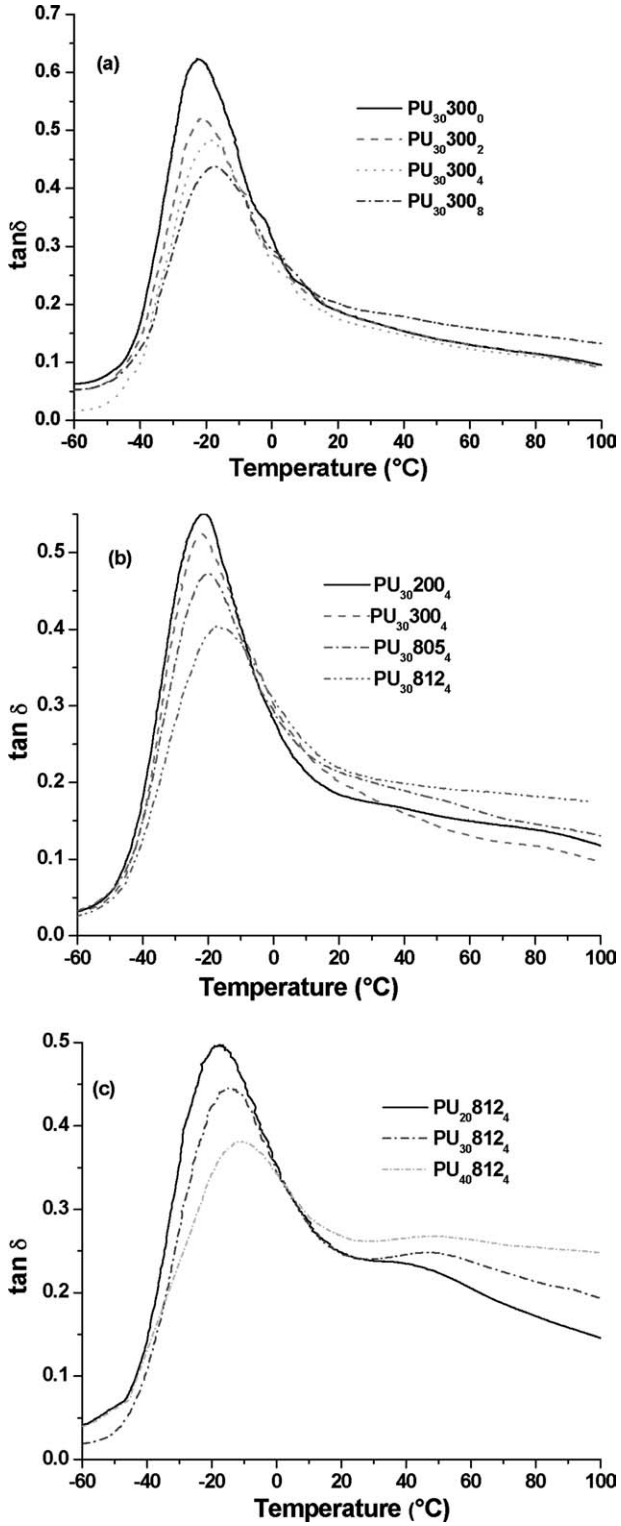

Figure 12. tan δ vs. temperature plots for different PU nanocomposites system varying with (a) nanosilica loading, (b) nature of nanosilica, and (c) microstructure of hyperbranched polyol.

hyperbranched polyol, more efficient anchoring takes place as a result of the presence of a higher number of hydroxyl groups. Obviously, higher T_g (−9°C) is observed for $PU_{40}812_4$ as compared to that of $PU_{30}812_4$ and $PU_{20}812_4$ (−12 and −17°C, respectively). This is in good agreement with the theoretical prediction for highly branched polymers and is analogous to the results on linear polymers[35]; i.e., longer arms yield higher glass

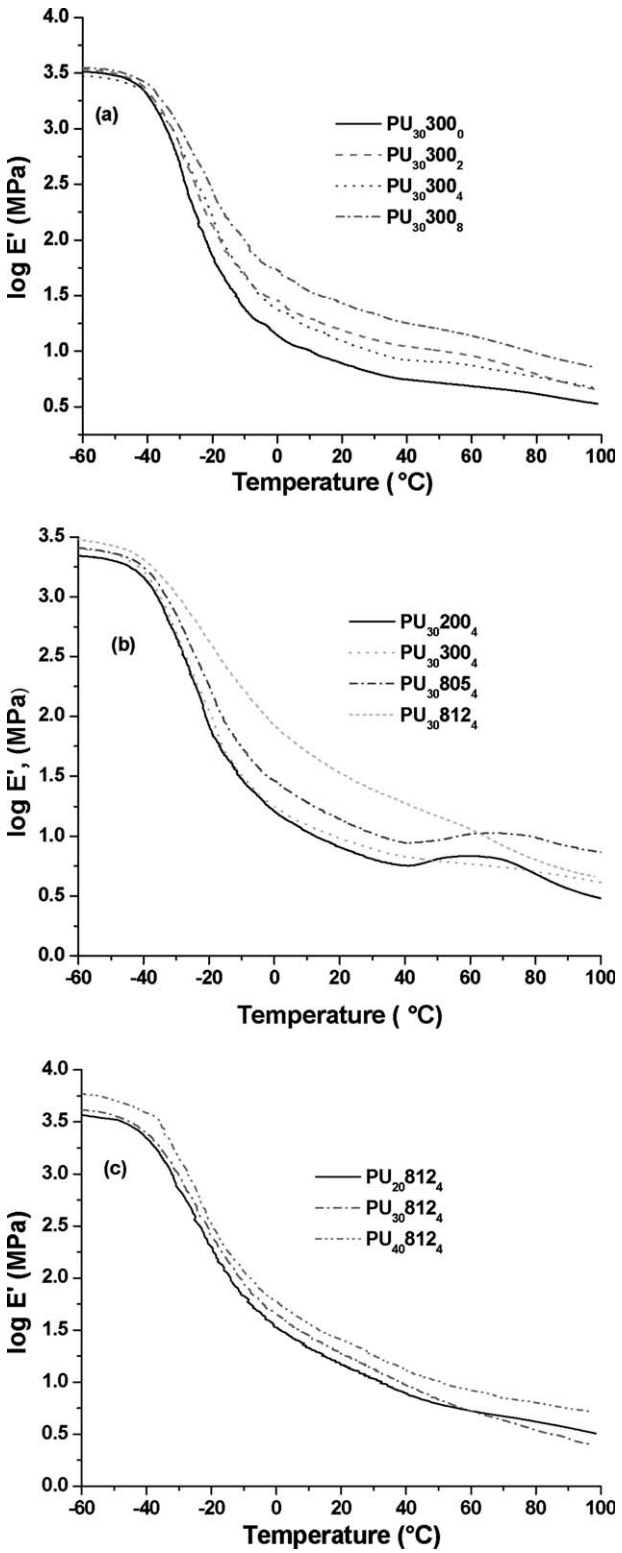

Figure 13. Storage modulus δ vs. temperature plots for different PU nanocomposites system varying with (a) nanosilica loading, (b) nature of nanosilica, and (c) microstructure of hyperbranched polyol.

Table IV. Dynamic Mechanical Properties of Different PU-Nanocomposites

Sample designation	T_g (°C)	tan δ_{max}	log E' (MPa)		
			−25°C	0°C	25°C
$PU_{30}300_0$	−22	0.62	2.26	1.13	0.79
$PU_{30}300_2$	−21	0.52	2.41	1.38	1.03
$PU_{30}300_4$	−19	0.48	2.42	1.46	1.11
$PU_{30}300_8$	−17	0.43	2.73	1.71	1.38
$PU_{30}200_4$	−21	0.55	2.31	1.24	0.82
$PU_{30}805_4$	−15	0.44	2.61	1.54	1.13
$PU_{30}812_4$	−12	0.40	2.71	1.61	1.27
$PU_{20}812_4$	−17	0.47	2.47	1.34	1.01
$PU_{40}812_4$	−9	0.37	2.81	1.80	1.41

relaxation temperatures. As whole, the increment of T_g is 13°C when $PU_{40}812_4$ is compared with $PU_{30}300_0$.

It is noticeable that the addition of nanosilica leads to an increase in the storage modulus consistent with the reinforcing action of the addition of the silica as filler [Figure 13(a)]. The storage modulus increases with the increase of silica concentration. As the temperature increases, the nanocomposites show a gradual drop in the storage modulus, as usual. The storage modulus of the nanocomposite film at 4 wt % loading ($PU_{30}300_4$) at 25°C is increased by 40%, over the pristine material of $PU_{30}300_0$. Ma et al.[36] show the same trend of an increase of the storage modulus in rectorite/linear thermoplastic PU nanocomposites. A higher storage modulus is observed for the treated silica nanocomposites [Figure 13(b)]. For example, $PU_{30}300_4$ has a logarithmic modulus value of 1.11 MPa, which is increased to 1.27 MPa for $PU_{30}812_4$ at 25°C. Our study also shows that the molecular weight of the hyperbranched polyester can have a significant effect on the viscoelastic properties of the cured PUs. The storage modulus value of $PU_{40}812_4$ is almost 78% higher than that of $PU_{30}300_0$. The T_g and storage modulus values increase as the molecular weight and the functionality increase [Figure 13(c)].

Thermogravimetric Analysis

Thermal stability of pristine PU and its nanocomposites from the untreated and the treated nanosilica at different loadings has been investigated by TGA. The degradation behavior of the nanocomposites is shown in Figure 14(a, c). A gradual weight loss is observed starting at around 260°C for all of the PUs. This initial weight loss is possibly due to the degradation of the hard segment present in the PU matrix, which continues for some period. Because the actual decomposition of the cured nanocomposites begins at elevated temperatures, the weight loss occurs at a faster rate.

The intersection point between the initial slope and the slope followed after the fast decomposition basically provides primary onset of the decomposition temperature (T_i). T_i values are directly computed by the TGA instrument. The samples containing nanosilica particles provide a higher T_i than the pristine PU. With an increase of the nanosilica loading, T_i increases. When compared with the silica loading, $PU_{30}300_8$ shows the

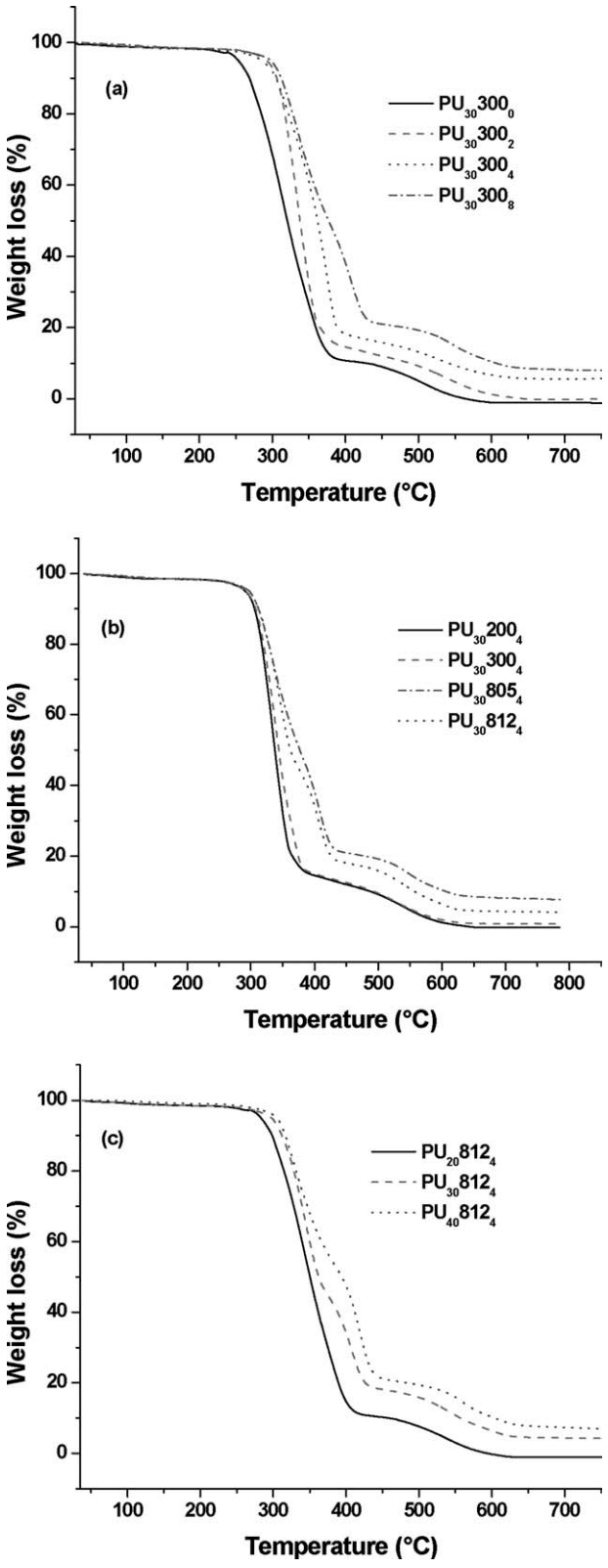

Figure 14. TGA thermogram of different PU nanocomposites system varying with (a) nanosilica loading, (b) nature of nanosilica, and (c) microstructure of hyperbranched polyol.

Applied Polymer SCIENCE

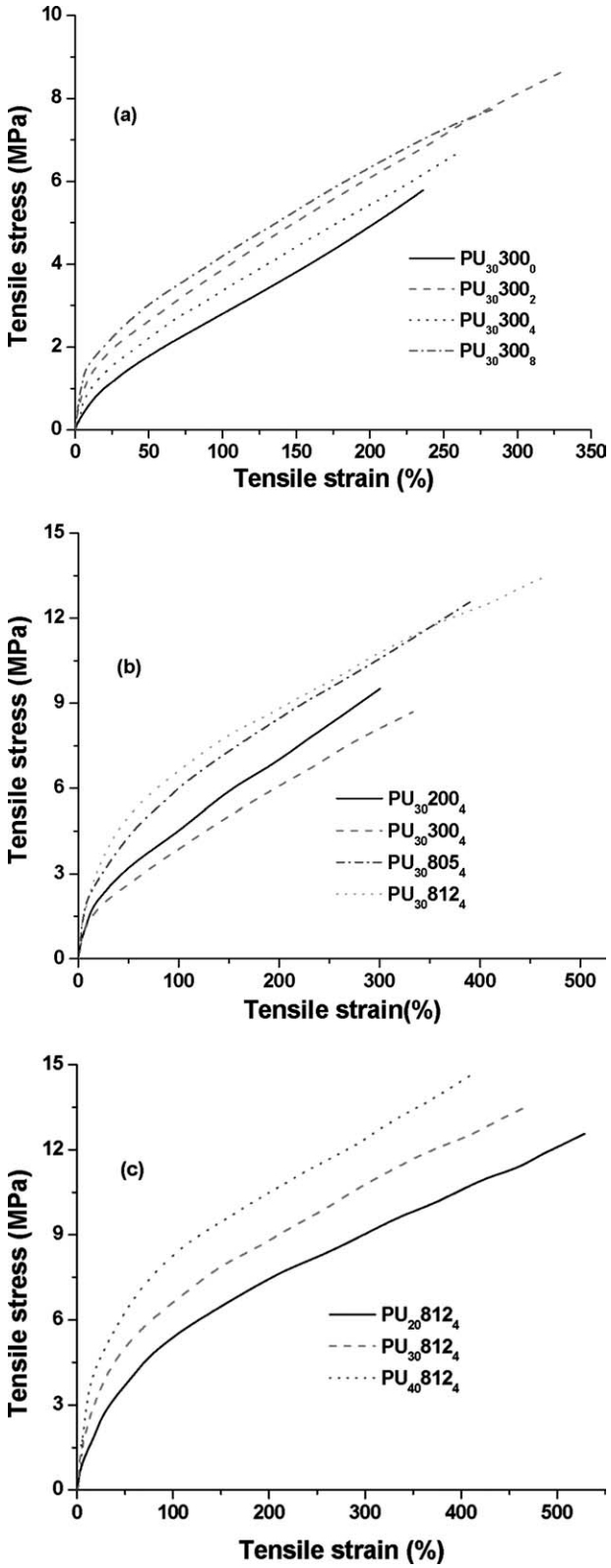

Figure 15. Tensile properties of different PU nanocomposites system varying with (a) nanosilica loading, (b) nature of nanosilica, and (c) microstructure of hyperbranched polyol.

highest thermal stability and its T_i and temperature at which maximum degradation occurs (T_{max}) are about 30 and 27°C, respectively, higher than those of the neat polyurethane. The rate of degradation is also lower than that of the pristine polyurethane, indicating higher thermal stability of the nanocomposites. This is due to the fact that the inorganic material can prevent heat and limit further degradation. In general, silica particles can enhance the thermal stability of the polymer by acting as the thermal insulator to the volatile products generated during decomposition.

The effect of nature of silica on the thermal stability is shown in Figure 14(b). Thermal stability can be increased with improving the dispersibility of nanosilica; so T_{max} of $PU_{30}812_4$ is about 7°C higher than those of $PU_{30}300_4$ due to good dispersibility of nanosilica (Figures 4 and 5) in PU nanocomposites. This increase in the thermal stability with an increase of generation of polyol could be due to increasing crosslinking owing to the availability of a higher number of end hydroxyl functional groups that take part in the crosslinking reaction.

Mechanical Properties

Representative stress–strain curves for the nanocomposites are depicted in Figure 15. Incorporation of silica nanoparticles in PU matrix leads to an increase in tensile strength and modulus, as shown in Figure 15(a). There is a 37% increase of 100% modulus with the addition of 4 wt % of nanosilica in PU_{30}. The tensile strength increases steadily up with 4 wt % silica loading (by 52% over pristine PU) before a decrease at higher loading. From the AFM investigations earlier section, it is observed that good dispersion is achieved up to 4 wt % silica loading. Above 4 wt % nanosilica loading, the formation of homogeneous nanostructure is difficult. The best tensile strength is observed for $PU_{40}812_4$ which is almost 155% higher than that of $PU_{30}300_0$. This is in agreement with the morphology study by AFM analysis. The homogeneous dispersion of silica particles shows an effective reinforcement effect for the polymer matrix. The nanodispersed silica affords a higher stress-bearing capability and efficiency. Stronger interactions between nanosilica and the polymer molecules associated with a larger contact surface result in effective constraint of the motion of the polymer chains. Because of the agglomeration of the nanofillers, the filler–filler interaction is predominant over the filler–polymer interaction. Also, agglomerated particles act as defects. As a result, a decrease in the tensile strength is observed in all of the nanocomposites containing 8 wt % nanosilica loading. When the mechanical properties are compared for the composites containing the treated and the untreated silica particles, the former one shows better properties [Figure 15(b)], as dispersion of the filler plays a great role in the properties of the nanocomposites. Figure 15(c) shows the effect of the number of functionalities of branched polyols with a fixed treated silica (Aerosil®R812S) loading (4 wt %) on the tensile strength of different PU nanocomposites. There is a 20% increase in the tensile strength of H40 cured 4 wt % Aerosil®R812S silica PU nanocomposites over the H20 cured PU silica nanocomposites. The superior tensile properties are attributed to the higher number of end —OH functionalities in the branched crosslinker molecules. The addition of the nanofillers has a synergistic effect on the tensile

properties of the PUs. With the addition of nanosilica, even the elongation at break of the PU nanocomposites increases. The elongation at break increases by 42% for $PU_{30}300_4$, over their pristine PUs at 4 wt % silica loading. The increase in the elongation at break is mainly due to the enhanced stress-bearing capability of the nanocomposites. It is to be noted that with an increase in the functionality in the hyperbranched polyol, the elongation at break increases in the PUs.

CONCLUSIONS

In this study, synthesis of nanocomposites involving reactive hyperbranched polyols, PU prepolymer, and nanosilica of different particle sizes and surface treatments was carried out. The nanocomposites provide thermally stable and mechanically strong materials. The nanosilica dispersion was characterized by atomic force microscopy, showing that nanosilica was homogeneously dispersed in the PU matrix at a low content of nanosilica (<4%). Approximately 52% increment in tensile strength, 40% increment in the storage modulus along with a improvement in thermal stability were observed with the addition of 4 wt % nanosilica over the pristine PU. At higher filler content, agglomeration of nanosilica resulted in inconsistent dispersion. The dispersion as well as the properties of PU nanocomposites was compared for the samples containing the treated and the untreated nanosilicas. It was shown that the organo-treated silica exhibited better thermal and mechanical properties than those containing the untreated one. The higher the level of functionality of the hyperbranched polyol, the higher is the property enhancement.

REFERENCES

1. Pattanayak, A.; Jana, S. C. *Polymer* **2005,** *46*, 5183.
2. Xu, R.; Manias, E.; Snyder, A. J.; Runt, J. J. *Biomed. Mater. Res.* **2003,** *64*, 114.
3. Zhang, J.; Manias, E.; Wilkie, C. A. *J. Nanosci. Nanotechnol.* **2008,** *8*, 1597.
4. Giannelis, E. P. *Adv. Mater.* **1996,** *8*, 29.
5. Maiti, M.; Bhowmick, A. K. *J. Polym. Sci. B Polym. Phys.,* **2006,** *44*, 162.
6. Yoo, Y.; Paul, D. R. *Polymer* **2008,** *49*, 3795.
7. Ganguly, A.; Sarkar, M. D.; Bhowmick, A. K. *J. Appl. Polym. Sci.* **2006,** *100*, 2040.
8. Sadhu, S.; Bhowmick, A. K. *J. Polym. Sci. B Polym. Phys.* **2004,** *42*, 1573.
9. Jiang, D.; Retsos H.; Giannelis, E. P. *Small* **2008,** *4*, 662.
10. Maiti, M.; Bhattacharya, M.; Bhowmick, A. K. *Rubber Chem. Technol.,* **2008,** *81*, 384.
11. Choi, Y. S.; Kim, T. K.; Kim, E. A.; Joo, S. H.; Pak, C.; Lee, Y. H. Chang, H.; Seung, D. *Adv. Mater.,* **2008,** *20*, 2341.
12. Qi, D.; Bao, Y.; Weng, Z.; Huang, Z. *Polymer* **2006,** *47*, 4622.
13. Aso, O.; Eguiazabal, J. I.; Nazabal, J. *Comp. Sci. Technol.,* **2007,** *67*, 2854.
14. Wu, C. L.; Zhang, M. Q.; Rong, M. Z.; Klaus Friedrich, K. *Comp. Sci. Technol.,* **2005,** *65*, 635.
15. Schollenberger, *S. C. US Patent 2,871, 218*, 1959.
16. Schollenberger, S. C. In Handbook of Elastomers, 2nd ed.; Bhowmick, A. K.; Stephens, H. L., Eds.; Marcel Dekker: New York, **2001;** Chapter 14, p 387.
17. Hepburn, C. Polyurethane Elastomers; Applied Science Publishers Ltd: England, **1982;** Chapter 2, p 27–48.
18. Buhleier, E.; Wehner, W.; Vogtle, F. *Synthesis* **1978,** *55*, 155.
19. Newkome, G. R.; Yao, Z.-Q.; Baker, G. R.; Gupta, V. K. *J. Org. Chem.* **1985,** *50*, 2003.
20. Vogtle, F.; Gestermann, S.; Hesse, R.; Schwierz, H.; Windisch, B. *Prog. Polym. Sci.* **2000,** *25*, 987.
21. Jannerfeldt, G.; Boogh, L.; Manson, J. A. *E. Polymer* **2000,** *41*, 7627.
22. Maji, P. K.; Bhowmick, A. K. *J. Polym. Sci. A Polym. Chem.,* **2009,** *47*, 731.
23. Jena, K. K.; Raju, K. V. *S. N. Ind. Eng. Chem. Res.,* **2008,** *47*, 9214.
24. Available at: www.aerosil.com; Access date on 15 November **2009.**
25. Kraus, G. J. *Appl. Polym. Sci.* **1963,** *7*, 861.
26. Luo, Z. P.; Koo, J. H. *J. Microsc.* **2007,** *225*, 118.
27. Luo, Z. P.; Koo, J. H. *Polymer* **2008,** *49*, 1841.
28. Luo, Z. P.; Koo, J. H. *Mater. Lett.,* **2008,** *62*, 3493.
29. Shanmugharaj, A. M.; Bhowmick, A. K. *Rubber Chem. Technol.* **2003,** *76*, 299.
30. Bandyopadhyay, A.; De Sarkar, M.; Bhowmick, A. K. *J. Polym. Sci. B Polym. Phys.* **2005,** *43*, 2399.
31. Tien, Y. I.; Wei, K. H. *J. Appl. Polym. Sci.* **2002,** *86*, 1741.
32. Maji, P. K.; Guchhait, P. K. *Bhowmick, A. K. J. Mater. Sci.* **2009,** *44*, 5861.
33. Mishra, J. K.; Kim, I.; Ha, C. S. *Macromol. Rapid Commun.* **2003,** *24*, 671.
34. Xiong, J.; Liu, Y.; Yang, X.; Wang, X. *Polym. Degrad. Stab.* **2004,** *86*, 549.
35. Asif, A.; Shi, W.; Shen, X.; Nie, K. *Polymer* **2005,** *46*, 11066.
36. Ma, X.; Lu, H.; Lian, G.; Zhao, J.; Lu, T. J. *Appl. Polym. Sci.* **2005,** *96*, 1165.